Resubmitted corrected manuscript

Volatile phase separation in silicic magmas at Bajo de la Alumbrera porphyry Cu-Au deposit, NW Argentina

Anthony C. HARRIS, Vadim S. KAMENETSKY, Noel C. WHITE and David A. STEELE*

Centre for Ore Deposit Research, University of Tasmania, Private Bag 79, Hobart, Tasmania, 7001, Australia [e-mail: A.Harris@utas.edu.au]

** Central Science Laboratory, University of Tasmania, Private Bag 74, Hobart, Tasmania, 7001, Australia*

Abstract: At the Bajo de la Alumbrera porphyry Cu-Au deposit, NW Argentina, several key textural elements preserve evidence for volatile separation. Interconnected miarolitic cavities, while being studied extensively in granites, have now been recognized in intrusions related to porphyry Cu mineralization. Pods of saccharoidal quartz are connected by narrow, anastomosing zones of graphic quartz–alkali feldspar intergrowths and ragged biotite (with lesser apatite and magnetite). Their connectivity can be as much as 15cm; however, more commonly, the interconnected miarolitic cavities are approximately 1 to 2mm across and 5cm or less, long. Features such comb-quartz layered textures and magmatic-hydrothermal veins (P veins), combined with aqueous fluid phase equilibria from fluid inclusions, better constrain physical models of exsolution. We interpret these textures in the context of vapour phase formation, coalescence and accumulation in an evolving silicic magma. Recognition of textures, such as the interconnected miarolitic cavities reported here, may provide a simple exploration tool for porphyry Cu deposits, helping explorers to recognize evidence for a potentially fertile intrusions.

Keywords: porphyry, copper, volatiles, magma, magmatic-hydrothermal, miarolitic cavities, comb quartz

1. Introduction

Porphyry ore deposits largely originate from magmatic volatile phases exsolved from silicic magma ascending through the Earth's crust, or as it convects and crystallizes at shallow crustal levels (e.g., Burnham, 1981; Candela, 1991; Hedenquist and Lowenstern 1994; Shinohara and Hedenquist, 1997). Decompression and crystallization causes an aqueous phase to separate, forming bubbles in the melt (Burnham 1979, 1981; Burnham and Ohmoto, 1980). These bubbles accumulate in the cupola of the magma body; intermittent fracturing of the carapace allows the

volatiles to be released to the adjacent wallrock. Despite this process being well constrained by numerical models (e.g., Shinohara and Hedenquist 1997) and experimental petrology (e.g., Candela and Holland, 1984; Candela, 1991, 1994; Webster, 1992; Metrich and Rutherford, 1992; Williams et al., 1995), physical evidence for the separation and accumulation of an aqueous volatile phase in rocks associated with porphyry Cu deposits has been limited.

The magmatic-hydrothermal transition in porphyry ore deposits has been previously studied from two perspectives. From a magmatic perspective, researchers have traced the evolution of the associated magma to the point of fluid loss. The chemical evolution has been traced, textures related to fluid loss have been identified (e.g., Dilles, 1987), and most recently, silicate-melt inclusions and co-existing aqueous phases, trapped in primary inclusions in phenocrysts, have been analyzed (Harris et al., 2003b; Kamenetsky et al., 1999; 2003). From the hydrothermal perspective, fluids related to different generations of veins, and to the associated hydrothermal alteration, have been characterized (e.g., Lowell and Guilbert, 1970; Gustafson and Hunt, 1975). The clearest evidence that some silicic magmas exsolve large volumes of aqueous fluids comes from geologic features; the occurrence of voluminous greisens, pegmatites, and the preservation of miarolitic cavities and comb-quartz layered textures in the carapace of some granites, while being extensively studied in Sn ± W-Bi and Mo granite-related systems (e.g., Jahns and Burnham, 1969; Kirkham and Sinclair, 1988; Candela and Blevin, 1995; Lowenstern and Sinclair, 1996) have only recently been documented in porphyry Cu systems (e.g., Kirwin and Seltmann, 2002; Lickfold et al., 2003).

Hydrothermal alteration in porphyry Cu deposits changes from early potassic (quartz-biotite-K-feldspar) through to late phyllic (quartz-sericite ± pyrite) alteration assemblages, with Cu mineralization being associated with the potassic assemblages. Numerous inclusion studies have found high temperature (up to 800°C), hypersaline (up to 70 wt% NaCl equivalent) fluid inclusions, which may coexist with vapor-rich liquid inclusion, are common in the potassic alteration assemblages (e.g., Eastoe, 1978; Haynes and Titley, 1980; Wilson et al., 1980; Ahmad

and Rose, 1980; Beane and Titley, 1981). More commonly, the fluid inclusions trapped in potassic alteration zones have cooled through a few hundred degrees (typically to between 350 and 500°C) from original magmatic temperatures and have been chemically modified from their primary compositions. Notwithstanding this, the calculated $\delta^{18}O$ and δD isotope compositions for fluids associated potassic alteration of the wallrock imply a magmatic origin (e.g., Sheppard and Gustafason, 1976).

We present detailed petrographic observations of interconnected miarolitic cavities and other primary igneous features, combined with silicate-melt and fluid inclusion studies (e.g., Harris et al., 2003a, b), from porphyritic intrusions at the Bajo de la Alumbrera deposit, NW Argentina. These textures preserve evidence of volatile exsolution (e.g., Kirkham and Sinclair, 1988; Lowenstern and Sinclair, 1996) and complete the continuum between magmatic and hydrothermal systems.

2. The Bajo de la Alumbrera Deposit

The Bajo de la Alumbrera deposit occurs in the Farallón Negro Volcanics, whose emplacement was part of one of the last magmatic events in the development of the Miocene magmatic arc of the central Andes. Magmatism in this district occurred ~200 km to the west of the Miocene magmatic arc during the Late Oligocene and Early Miocene. It was focused in a crustal scale arc-oblique deformation zone (de Urreiztieta et al., 1996), referred to as the Tucuman Fault Zone, that represents a major boundary between a physico-tectonic plateau (the Puna-Altiplano) and a basement-uplift terrane (Fig. 1). Uplift of the crystalline basement rocks occurred synchronous with, or immediately before, the onset of regional volcanism during the Middle Miocene; both uplift and volcanism have continued intermittently to the Recent (Jordan and Allmendinger, 1986; Tabbutt et al., 1987; Reynolds et al., 1987; Ramos et al., 1988; Strecker et al., 1989, 1990; Coughlin et al., 1998). The district is an intermontane basin that lies in a structural fault-block depression in this linear deformation zone.

The Bajo de la Alumbrera deposit is a Au-rich porphyry Cu system that contains 402 × 10^6 t averaging 0.54% Cu and 0.64 g/t Au (pers. comm., D. Keough, 2001). The bulk of the Cu-Fe sulfides occur in pervasive and fracture-controlled potassic (biotite-K-feldspar-quartz±magnetite) alteration assemblages that overprint several porphyritic phases that have intruded volcanosedimentary rocks (Ulrich and Heinrich, 2002; Proffett, 1997, 2003; Harris et al., 2004). At least five high-K calc-alkaline (to shoshonitic) plagioclase-biotite (hornblende)-phyric dacite, trachydacite, trachyandesite, and andesite porphyries occur (Fig. 2; Stults, 1985; Müller and Forrestal, 1998; Sasso and Clark, 1998; Ulrich and Heinrich, 2002). The mineralized porphyry intrusions were emplaced in the latest Miocene, between 8.02 ± 0.14 and 7.10 ± 0.07 Ma ($^{206}Pb/^{238}U$ zircon ages; Harris et al., 2004). Total fusion and step-heating $^{40}Ar/^{39}Ar$ geochronology reveals that the intrusions cooled through the Ar-retention temperature of biotite (ca. 310°C: McDougall and Harrison, 1999) between 7.10 ± 0.13 and 6.83 ± 0.07 Ma (Sasso and Clark, 1998).

Individual porphyritic intrusions are up to several hundred metres wide (Fig. 2) and extend up to about a kilometre in known vertical extent (Fig. 2; Proffett, 1997, 2003; Ulrich and Heinrich, 2002). Phenocrysts vary in abundance between 20 and 30 volume percent (vol %), consisting of abundant medium- to coarse-grained (up to 5 mm) plagioclase (<30 %), with lesser quartz (<5 mm, <15 %), biotite (<5 mm, <5%) and hornblende (2-3 mm, <2 %); the groundmass is quartzo-feldspathic (Fig. 3). A minor amount of alkali feldspar also occurs as phenocrysts in the late intrusions. Apatite, zircon, magnetite and titanite occur in trace quantities as discrete microphenocrysts and as inclusions in various phenocrysts.

The zone of intense and texturally destructive hydrothermal alteration at Bajo de la Alumbrera is up to 3 km across. Most disseminated Cu-Fe sulfide and Au mineralization occurs in the potassic (biotite, K-feldspar and lesser quartz) alteration zone (J. M. Proffett *writ. comm.* 2001; Ulrich and Heinrich 2002). Propylitic (chlorite-illite-epidote-calcite) assemblages (Stults,

1985; Guilbert, 1995) rim this zone and are cut by magnetite (± quartz -biotite) veins. In the core of the deposit, magnetite-quartz veins become increasingly abundant (J. M. Proffett *writ. comm.* 2003). Intermediate argillic (chlorite-illite ± pyrite) alteration overprinted the potassic zone and appears in part to be synchronous with the outermost phyllic alteration. Phyllic (quartz-muscovite-illite±pyrite) alteration occurs across the top of the deposit and extends downwards along the periphery of the potassic alteration zone. Fault and fracture-fill, carbonate-base metal assemblages resulted from the final hydrothermal phase in the deposit.

Calculated $\delta^{18}O$ and δD fluid compositions and fluid inclusion studies reveal that high temperature (up to 825°C) and saline (over 30 wt% NaCl equivalent) magmatic fluids were responsible for the potassic alteration assemblages (Ulrich et al., 2002; Harris et al., 2003b). Lower temperature (<350°C) and less saline (<15 wt% NaCl equivalent) magmatic fluid and/or admixtures with meteoric water produced the late-stage chlorite-illite-rich assemblages (Ulrich et al., 2002).

3. Intrusion petrography

Based on precise mapping and detailed observations, Proffett (1995; 1997; 2003) constrained the intrusion history at Bajo de la Alumbrera (Ulrich and Heinrich, 2002). Geochronologic work has divided the five or more porphyritic intrusions into two temporally distinct events: one group emplaced at ca. 8.0 Ma (early porphyries) and another intruded about a million years later (late porphyries; Harris et al., 2004). Although both are associated with varying degrees of hydrothermal alteration (Proffett, 2003), the bulk of the Cu-Au mineralization is apparently associated with the younger group of porphyries. The highest Cu grades appear to rim and overprint the margins of the so-called P3 group of porphyries (Fig. 2; Ulrich and Heinrich, 2002; Proffett, 2003).

3.1 Early porphyries

Despite uncertain field relationships (Ulrich and Heinrich, 2002; Proffett, 2003), the oldest porphyritic intrusion in the deposit is thought to be the Northeast Porphyry (Fig. 2). Proffett (2003) states that, where seen the NE Porphyry is cut by all hydrothermal alteration stages. The Los Amarillos Porphyry is the oldest temporally constrained intrusion in the deposit (8.02 ± 0.14 Ma; Harris et al., 2004). Despite intense texturally destructive alteration assemblages obscuring primary igneous textures, the Los Amarillos Porphyry in part appears as an igneous breccia (Proffett, 2003). Moreover, where observed it appears to be plagioclase-phyric (up to 20 %), with equal proportions of biotite and hornblende (between 5 and 10 %) and quartz (up to 3 %); the groundmass is cryptocrystalline (Ulrich and Heinrich, 2002). Rounded quartz phenocrysts and angular quartz vein fragments occur throughout.

The P2 (or Colorado Norte) Porphyry is the main mineralizing intrusion of the early group of porphyries at Bajo de la Alumbrera (Fig. 2). Based on field relationships, subsequently confirmed by U-Pb zircon geochronology (7.98 ± 0.14 Ma; Harris et al., 2004), Proffett (2003) mapped the P2 Porphyry as being younger than the Los Amarillos Porphyry. The P2 Porphyry is more strongly altered and mineralized than any other porphyry at Bajo de la Alumbrera (Proffett, 2003). K-feldspar-biotite and quartz alteration assemblages obscure the primary igneous textures and mineralogy, which can locally be seen to be plagioclase-phyric dacite with minor biotite and hornblende phenocrysts. Plagioclase (<5 mm; 10 to 25 %) occurs as subhedral and broken phenocrysts. Proffett (1997, 2003) describes biotite books (1 to 3 mm; <3 %); however, biotite more commonly occurs with magnetite as irregular clots. Large (up to 6 mm) quartz eyes occur in the P2 Porphyry (Proffett, 2003). Other phases include minor apatite and magnetite with trace amounts of zircon. The groundmass comprises crystals (< 0.1 mm) of feldspar and a lesser amount of quartz.

3.2 Late porphyries

The Early P3 porphyries (including the Quartz Eye Porphyry) are a group of biotite- and plagioclase-phyric dacites (Proffett, 1997) emplaced at 7.10 ± 0.07 Ma (Harris et al., 2004).

They formed one of the largest intrusive events at Bajo de la Alumbrera (Proffett, 2003). In these porphyries, plagioclase (typically 1-3 mm; <40 %) occurs as twinned and distinctly zoned euhedral phenocrysts. Coarser (up to 5 mm) 'megacrysts' of plagioclase are rare: these comprise several subhedral plagioclase crystals. Plagioclase poikilitically encloses small biotite laths. Biotite phenocrysts (1-7 mm; <3 %) occur as books that enclose euhedral plagioclase, quartz, titanite and magnetite. Biotite also occurs as irregular clots with magnetite, chalcopyrite and quartz (Proffett, 1997, 2003). Hornblende is rare, or, more commonly, absent. Quartz eyes (1-4 mm) are rare and irregularly shaped, with ragged edges. Rare alkali feldspar (<1 mm) phenocrysts occur. The groundmass is cryptocrystalline to very fine-grained (<0.2 mm), and comprises quartz and feldspar.

The Late P3 porphyries (including the Campamiento and North porphyries) are a group of hornblende- and plagioclase-phyric dacites that contain distinctive euhedral 'book' biotites and biotite (-magnetite) clumps (Proffett, 1995, 1997; Ulrich and Heinrich, 2002). Megacrysts of plagioclase (<5 mm; <25 %) occur as subhedral and euhedral twinned clusters that contain small (<0.25 mm) biotite laths, hornblende and magnetite. These megacrysts appear rounded. Isolated euhedral oscillatory-zoned plagioclase (<5 %) also occurs. Biotite (<3 mm; <5 %) and hornblende (<5 mm; <3 %) phenocrysts poikilitically enclose small crystals of plagioclase, apatite, and zircon. Hornblende is typically subhedral. Despite being rare, quartz eyes in the Late P3 porphyries are distinctive (Proffett, 2003): they are square shaped with rounded edges, or are embayed and apparently resorbed, giving them an ameboid appearance. Alkali feldspar (<2 mm; <2 %) phenocrysts are anhedralsubhedral to euhedral and occur in some phases of the Late P3 Porphyry. The aphanitic groundmass comprises quartz and feldspar. Small anhedral to subhedral apatite and zircon crystals are dispersed through the groundmass.

Other phases petrographically similar to the Late P3 porphyries include the Northwest and Post-Mineralization dykes (Proffett, 1997, 2003; Ulrich and Heinrich, 2002). Quartz eyes (average 2-5 mm; <5%) are distinctly larger (up to 10 mm), have an ameboid appearance, and

are embayed with pods of holocrystalline groundmass. Quartz poikilitically encloses hornblende, quartz, apatite, and zircon. Angular and rhomboid quartz phenocrysts are also common. Zoned and twinned euhedral plagioclase phenocrysts (average ~0.5 mm, up to 3 mm; 15%) are in part mantled by alkali feldspar. Alkali feldspar (<2 mm) phenocrysts are rare. Hornblende (<0.5 mm; <5%) occurs as euhedral prismatic laths that have distinct crystal boundaries and enclose apatite and plagioclase. Other phenocrysts include magnetite, titanite, apatite and zircon. Typically, the groundmass of these late stage porphyries is cryptocrystalline.

3.3. Hydrothermal alteration assemblages

Secondary potassic assemblages comprising biotite, K-feldspar, magnetite and quartz affect most porphyritic intrusions, modifying phenocrysts and obscuring primary igneous textures. Proffett (1997, published 2003) provided the first detailed macroscopic description of the potassic alteration assemblages: his study described zones rich in K-feldspar and others dominated by biotite. In the mineralized porphyries, K-feldspar-dominant assemblages comprise pervasive K-feldspar replacement of groundmass and phenocrystic feldspars, and where it is most intense occurs as a mosaic intergrowth of K-feldspar-quartz ± magnetite. Elsewhere, this alteration comprises clots of K-feldspar surrounded by a corona of fine K-feldspar-muscovite-quartz-apatite and biotite phenocrysts replaced by K-feldspar-muscovite ± magnetite. In zones dominated by biotite, phenocrystic biotite is commonly recrystallized, whereas fine-grained clumps of shredded biotite partially pseudomorph hornblende. Fine-grained biotite also occurs dispersed throughout the groundmass (Fig. 4). In part, the groundmass feldspars are altered to a mosaic of K-feldspar ± biotite-quartz-chlorite-rutile-apatite. Secondary magnetite occurs as disseminations intergrown with shredded biotite (Fig. 4B).

4. Primary Igneous Textures

Widespread texturally destructive pervasive hydrothermal alteration assemblages commonly overprint intrusions in porphyry Cu deposits, making it difficult to recognize phenocryst mineralogy and subtle primary igneous textures. Despite this, detailed microscopic

observation the porphyritic intrusions at Bajo de la Alumbrera has identified several textures providing critical evidence of the magmatic-hydrothermal transition.

4.1. Quartz eyes

There are two petrographically distinct types of quartz eyes in the mineralized porphyries (Fig. 5; Harris et al. 2003a). Type 1 consists of typical quartz phenocrysts (Fig. 5A); they are large (up to 8 mm in diameter), rounded and irregular anhedral crystals. Individual crystals are dispersed throughout the groundmass, and may have distinct crystal edges, and contain small inclusions of feldspar and magnetite. Some quartz phenocrysts are embayed and apparently resorbed, giving them an amoeboid appearance (Fig. 5B). Type 1 quartz eyes occur in most porphyry phases.

Type 2 quartz eyes are elliptical, small (<2 mm), and consist of sugary aggregates of anhedral quartz crystals (Fig. 5C). They are distinctly different from quartz phenocrysts. Crystals of feldspar and magnetite are intergrown with the quartz. Some type 2 quartz eyes have empty voids in the core. Although mostly randomly distributed throughout the groundmass, type 2 quartz eyes may exhibit an apparent linear arrangement. They are surrounded by groundmass, and are not related to microfractures controlling hydrothermal alteration. They are interpreted to be miarolitic pods (e.g., Jahns and Burnham, 1969) or cavities (e.g., Candela and Blevin, 1995). Type 2 quartz eyes occur in both the P2 and P3 porphyries. Angular quartz vein fragments also occur in several of the intrusions at Bajo de la Alumbrera (e.g., Proffett, 1997, 2003). The quartz vein fragments are elongated, angular fragments with commonly distinct comb-tooth texture and laminated structure, and are distinct from the concentrically zoned quartz pods.

4.2. Interconnected miarolitic cavities

Narrow, anastomosing zones of graphic quartz–alkali feldspar intergrowths and ragged biotite (with lesser apatite and magnetite) connect some type 2 quartz eyes (Fig. 6) – this connectivity can be observed over as much as tens of centimetres. More commonly, these interconnected miarolitic cavities are approximately 1 to 2 mm across and 5 cm or less in length.

They exhibit a clear zonal arrangement, which has been referred to as a two-domain or 'double-bunger' texture (Candela and Blevin, 1995). The outer rim of these zones is characterized by fine (<0.2 mm) saccharoidal quartz–alkali feldspar and graphic quartz–alkali feldspar intergrowths. Randomly oriented and ragged biotite laths (with interlayered chlorite along the original biotite cleavage) also define the outermost margins of these zones. Coarser grained (0.2 to 0.5mm) aplite, composed of alkali feldspar and quartz with lesser biotite, occurs along the centre of the miarolitic cavities (Fig. 7). In part, large (up to 1 mm) alkali feldspar and quartz crystals clearly overgrow euhedral plagioclase phenocrysts – this includes myrmekitic quartz intergrown into plagioclase, to near complete overgrowth of plagioclase by K-feldspar (Fig. 7). In the latter case, sieve textured plagioclase is observed. Myrmekitic biotite in contact with K-feldspar demonstrates a primary magmatic origin for the associated shredded biotite.

Scanning electron microscopy reveals that the voids of the miarolitic cavities are lined with a complex mineral assemblage of euhedral crystals (Fig. 8). Quartz and magnetite are distinctive, with euhedral terminations into the voids (Fig. 8A). The bases of these crystals, however, are irregular and seriate, apparently overgrowing phenocrysts. Biotite is similarly nucleated on the cavity's walls. It appears that euhedral apatite is loosely adhered to the walls of the voids (Fig. 8B). In part, very fine (2 to 5 _m, up to 30 _m), euhedral alkali feldspars surround the apatite and may help cement the apatite to the cavity's walls (Fig. 8D). Euhedral crystals of chalcopyrite occur amongst the fine alkali feldspars (Fig. 8E).

Interconnected miarolitic cavities have been found in the P3 group of porphyries. The best example of this texture thus far is in Minera Alumbrera diamond drill hole 50-46.43 from 613.2 m depth.

4.3 Comb quartz layered textures

Comb quartz layered textures (also referred to as unidirectional solidification textures) have been found poorly developed along contacts of several porphyritic intrusions. At Bajo de la Alumbrera these textures define alternating bands (5 to 20 mm thick) of fine- to coarse-grained

prismatic quartz (Fig. 9), and radial intergrowths of biotite and sugary quartz-feldspar. Apical terminations of the quartz crystals are oriented perpendicular to the intrusion contact. Some quartz layers have a wavy texture. Very fine-grained quartz intergrowths along the innermost contact of the related intrusion, give the texture a diffuse appearance.

Despite the quartz in comb quartz layered textures appearing optically continuous, cathodoluminescence (CL) imaging (Fig. 9) reveals internal complexity: well-defined luminescence band of varying widths commonly define concentric growth zones in coarse-grained prismatic quartz. Some quartz in the comb-quartz layered textures shows equant bipyramidal (or rare hexagonal) growth forms (Fig. 9B). Re-entrants and in some cases embayments, along with irregular overgrowths, imply resorption. This quartz morphology, especially the distinct equant bipyramids, is consistent with it being high-temperature _-quartz commonly observed in subvolcanic intrusions (Lowenstern and Sinclair, 1996).

4.4. Aplite vein dykes and transitional magmatic-hydrothermal quartz veins

Thin (<2 cm wide) and irregular fracture-controlled aplite-filled veins – referred to as 'vein dykes' (e.g., Carten et al., 1988; Kirkham and Sinclair, 1988) – of saccharoidal alkali feldspar and quartz cut P2. The aplite is characterized by myrmekitic intergrowths of alkali feldspar and quartz. Magnetite (and rare chalcopyrite) is disseminated throughout. Vein dykes have also been found in the P3 group of porphyries.

Some of the earliest Cu mineralization at Bajo de la Alumbrera occurs in diffuse quartz-sulfide veins that cut the mineralized porphyries. The veins are texturally similar to those described as A veins (El Salvador, Chile; Lowell and Guilbert, 1970). Typically, these veins consist of saccharoidal quartz, with minor amounts of K-feldspar ± hornblende-biotite-magnetite. Chalcopyrite (and rare pyrite) also occurs throughout. Some quartz crystals are distinctly prismatic, with primary fluid inclusion trails defining growth bands in individual quartz crystals. CL imaging of quartz highlights its sugary nature in these transitional veins (Fig. 9D; cf. images presented by Penniston-Dorland, 2001). Furthermore, the CL imaging reveals

well-defined concentric growth zoning of varying widths, overgrowths and embayments in equant bipyramidal quartz crystals; i.e., high-temperature _-quartz. Unusually high Cu concentrations of some aqueous inclusions, combined with the recognition of silicate-melt inclusions in these veins, suggest that these are the earliest transitional magmatic-hydrothermal veins at Bajo de la Alumbrera. As such, they have been referred to as P veins, reflecting their primitive role in the evolution of this deposit (Harris et al., 2003b). They have been observed to cross cut the P2 and P3 group of porphyries.

5. Magmatic Inclusion Populations

The silicate-melt and fluid inclusion populations present in both types of quartz eyes, comb-quartz layered textures, and magmatic-hydrothermal transitional veins (P veins) are similar. Two populations of silicate-melt inclusions are recognised (Table 1). Volatile-rich silicate inclusions are most common, and have an negative crystal form (Fig. 10A). Room temperature observations reveal small angular, crystalline silicate aggregates throughout: they vary mostly between 5 and 35 μm in diameter. A brine phase also occurs – this brine portion of the silicate-melt inclusion becomes visible following prolonged heating (Fig. 10B; see micro-thermometry experiments below). A vapor bubble (20-40 vol% vapor) is normally present. These composite inclusions contain several opaque phases (possibly chalcopyrite and magnetite). The second and less abundant silicate-melt inclusion population lacks the salt phase so prominent in the volatile-rich group IA inclusions (Table 1); these inclusions have a negative crystal or spherical shape and contain a vapor bubble (between 20 and 60 vol%). Their size varies mostly between 15 and 45 μm, rarely up to 60 μm. Opaque daughter crystals (magnetite and chalcopyrite) are rare.

In the type 1 quartz eyes, silicate-melt inclusions coexist with vapour-rich and hypersaline liquid-rich inclusions (Fig. 10C): the later inclusions containing numerous daughter minerals including halite, anhydrite, chalcopyrite and magnetite (Table 1). Little to no liquid is visible. Vapour-rich inclusions (Table 1) are larger but less abundant when associated with the

hypersaline liquid-rich inclusions. Some quartz phenocrysts, especially in the earliest porphyry phases, are characterized by vapour inclusions only. Silicate-melt inclusions in the type 2 quartz eyes coexist with brine inclusions that have a higher proportion of liquid. Moreover, they are crowded with halite-anhydrite ± magnetite -sylvite-chalcopyrite and numerous unidentified phases. Similar inclusion assemblages exist in comb-quartz layered textures (Fig. 10D to G). Coexisting vapor-rich inclusions are rare in either case. Rare hypersaline liquid-rich inclusions from the comb-quartz layered textures have distinct apatite crystals that coexist with halite, making this crystal assemblage similar to that observed in interconnected miarolitic cavities. Typically the hypersaline liquid-rich inclusions in the quartz eyes and comb-quartz layers are petrographically similar to those found in the earliest potassic alteration at Bajo de la Alumbrera (Ulrich et al., 2002; Harris, 2002).

Silicate-melt inclusions in the P veins are similar to those in quartz phenocrysts (Harris et al., 2003b). Typically, the melt inclusions have a negative crystal shape or are spherical and contain a vapor bubble (between 20 and 40 vol%), along with numerous silicate, salt, sulfide and oxide crystals (Fig. 10H). Minor amounts of liquid are also associated with the salt crystals. The inclusion size varies mostly between 5 and 25 μm, up to 45 μm. Opaque daughter crystals, including magnetite and chalcopyrite occur throughout. Vapor-rich and hypersaline liquid-rich inclusions (5 to 35 μm) coexist with the silicate-melt inclusions. The vapour-rich inclusions commonly form elongate ellipsoidal inclusions or negative crystal shapes with up to 90 vol% vapor and may contain one opaque phase. Hypersaline liquid-rich inclusions are ellipsoidal or have negative crystal shapes; they are typically crowded with crystals, including halite, and less commonly sylvite (Fig. 10I). Anhydrite, biotite, hornblende, apatite and rutile are also found in these inclusions. Their triangular shape distinguishes chalcopyrite crystals, and microanalysis shows the presence of magnetite; there are also several other as yet unidentified opaque phases.

5.1. Silicate-melt and fluid inclusion microthermometry

Homogenization experiments on silicate-melt and fluid inclusions were performed at 1-atm external pressure using a LINKAM TS1500 heating stage. When individual quartz crystals are heated to 800°C for several hours and then quenched, a homogenous silicate glass is produced from the crystalline silicate aggregates. Cooling and quenching of the silicate-melt inclusions reveal spherical globules (<1 to 8 μm), consisting of salt crystals and vapour bubbles (Harris et al., 2003a, b) – they are morphologically similar to hypersaline liquid inclusions typically found in potassic alteration assemblages (e.g., Ulrich et al., 2002).

Microthermometric experiments reveal that for the silicate-melt inclusions in quartz eyes (type 1 and 2), the first dissolution of the salt phases occurs by 165°C, and is typically completed by 450°C, whereas vapour bubble disappearance in the brine component is as high as 550°C (Harris et al., 2003a). The minimum trapping temperature of the silicate-melt inclusions ranges from 750°C to 780°C, based on extended furnace-based heating experiments on the volatile-poor melt inclusions (Harris et al., 2003a). Adjacent polyphase brine inclusions also homogenise at high temperatures (615°C to 695°C; by vapour disappearance). Assuming a simple NaCl-H_2O system, the calculated salinities of the inclusions average 45 wt% NaCl equivalent (Bodnar et al., 1995).

Hypersaline liquid-rich inclusions trapped in the comb-quartz layered textures exhibit homogenisation by halite dissolution; i.e., vapour disappearance occurs between 315°C and 365°C, whereas the large halite typically disappears by 405°C. The true trapping temperature must have been much higher (> 573°C), given that these inclusions were trapped during the growth of equant bipyramids of _-quartz. These phase changes, combined with experimental data, indicate that the salinity is between 45 and 47 wt% NaCl equivalent (Cline and Bodnar, 1994). Reconstruction of the pressure-temperature trapping conditions (following the procedure outlined by Cline and Bodnar, 1994), confirm that these inclusion fluids were probably trapped

at pressures ≥0.7 kbar. By contrast, the majority of fluid inclusions from most vein and alteration stages at Bajo de la Alumbrera record fluid pressures of 0.3 kbar (Ulrich et al., 2002).

Microthermometry experiments on silicate-melt inclusions in the transitional magmatic-hydrothermal P veins reveal the dissolution of salts occurs between 105 and 560°C; whereas the melting of silicate phases occurs between 650°C and 765°C (Harris et al., 2003b). Minimum trapping temperatures of the silicate-melt inclusions is estimated at between 750°C and 800°C. Like silicate-melt inclusions in both types of quartz eyes, those found in the transitional magmatic-hydrothermal veins have spherical globules crowded with salts, vapor bubbles (<4 μm), and aqueous liquid.

Microthermometric experiments on primary hypersaline liquid-rich inclusions immediately adjacent to the silicate-melt inclusions (i.e., clearly coeval) in the P veins has found that salt dissolution is completed by 540°C, with homogenization by vapor disappearance occurring up to 845°C (Harris et al., 2003b). The calculated salinities of the inclusions are high, up to 53 wt% NaCl equivalent (but salinities were reported as high as 62 wt% NaCl equivalent; Ulrich et al., 2002), implying a magmatic origin, consistent with their temperature. Non-destructive, in-situ microanalysis by PIXE reveals usually high Cu concentrations, up to 10 wt%, in some of these hypersaline liquid-rich inclusions (Harris et al., 2003b).

6. Discussion

The clearest evidence that some silicic magmas exsolve large volumes of magmatic aqueous fluids comes from geologic features, such as the occurrence of voluminous greisens, and the preservation of miarolitic cavities (e.g., Candela and Blevin 1995) and comb quartz layered textures in the carapace of some granites (e.g., Lowenstern and Sinclair 1996). In porphyry Cu deposits, features such as interconnected miarolitic cavities may have been previously overlooked because of intense texturally destructive hydrothermal alteration. Their recognition at

Bajo de la Alumbrera, combined with aqueous fluid phase equilibria from inclusion microthermometry, provide important constraints for the magmatic-hydrothermal transition.

6.1. Exsolution and degassing of magmatic volatile phase

The potential for a crystallizing upper crustal silicic magma (with a sufficiently high water content) to form an ore deposit depends on the availability of metals in the magma, whether they partitioned into the magmatic volatile phase, and the history of the fluid after release from the magma chamber. At Bajo de la Alumbrera, the presence of biotite and/or hornblende phenocrysts in the dacites implies that the magma related to mineralization had between 2 and 5 wt.% water (Burnham, 1979). However, this value could have been as much as 8 wt.% (Johnson et al., 1994; Lowenstern, 1995). Only a relatively small amount of chloride is needed to lower the concentration of water necessary for saturation (Webster, 1997), so a large proportion of the water in the magma was available to form separate aqueous phases.

Most silicate-melt inclusions reported here are composite in nature; i.e., they are not homogenous, but contain small globules crowded with salt crystals, vapor bubbles and an aqueous liquid. In essence, these inclusions represent the original entrapment of melt plus a magmatic volatile phase (Harris et al., 2003a, b); i.e., they represent heterogeneous trapping of phases immiscible at magmatic or near-magmatic conditions (e.g., Frezzotti, 1992; Roedder, 1992; Yang and Bodnar, 1994). PIXE microanalysis indicates that the highest concentrations of Cu, Zn, and Pb reside in the Cl-rich fluid phase of the silicate-melt inclusions (Harris et al., 2003b). This finding is consistent with that anticipated by numerical models (Candela and Holland, 1984; Candela, 1989; Metrich and Rutherford, 1992; Bodnar, 1995; Candela and Piccoli, 1995; Williams et al., 1995), in that metals are preferentially partitioned into the magmatic volatile phase rather than the silicate melt.

The stable phenocrystic assemblage quartz + magnetite + titanite in the mineralized porphyries indicates conditions that are more oxidizing than the nickel-nickel oxide (NNO) buffer + 2 log unit of oxygen fugacity (e.g., Nakada, 1991). Under conditions more oxidized than

NNO +1 log unit, most of the sulfur in the magma is in its most oxidized valence state (S^{+6}) as sulfate (SO_4^{2-}), thus stabilizing anhydrite as a phenocrystic phase (Carroll and Rutherford, 1987). The absence of anhydrite from the mineralized dacitic intrusions implies the loss of magmatic sulfur to an exsolved aqueous fluid, as sulfur is preferentially partitioned into a fluid over the silicate melt from which these fluid phases were exsolved (Pasteris, 1996) – this is consistent with occurrence of anhydrite in the fluid inclusions from the P veins (Harris et al., 2003b).

6.2. Controls on exsolution of magmatic volatile phase

Reconstruction of the volcanic architecture above Bajo de la Alumbrera suggests that the source magma body occurred well below 3 km (≥ 0.7 kbar lithostatic pressure; Harris, 2002; Harris et al., 2003). Pressure estimates based on aqueous phase equilibria from fluid inclusions in the earliest vein stages are consistent with this (Ulrich et al., 2002; Harris et al., 2003b). Provided the source magma had a pressure less than the critical pressure of a simple NaCl-H_2O system (i.e., 800°C at ~1.5 kbar; Knight and Bodnar, 1989), hypersaline liquid and vapor exsolved directly from the magma (e.g., Lowenstern et al., 1991; Lowenstern, 1995; Cline and Bodnar, 1994; Shinohara, 1994; Bodnar, 1995). This finding is implicit in the silicate-inclusions from most primary igneous textures; i.e., they typically contain spherical (<1 to 8 μm) hypersaline liquid globules (Harris et al., 2003b). Isolated magmatic inclusions represent homogenous trapping of silicate-melt, hypersaline liquid and less commonly vapor. Kamenetsky et al. (2003) stated that these inclusions confirm that volatiles (both hypersaline liquid and vapor) coexisted with the melt, and imply that the hypersaline liquid and vapor were independently but simultaneously separated from the magma.

An alternative model (e.g., Cline and Bodnar, 1994) involves the production of a hypersaline liquid and an accompanying vapor via aqueous phase separation of an originally low-salinity fluid (<10 wt% NaCl equivalent; referred to as 'supercritical' fluid) exsolved at 1.0 kbar pressure and 680°C (e.g., Hedenquist et al., 1998). At these conditions, Cline and Bodnar

(1994) show that a hypersaline liquid with a salinity of 45 wt% NaCl equivalent would be produced. Notwithstanding this, the abundance of composite silicate-melt inclusions (i.e., those that trap both melt and magmatic volatile phase) coeval with hypersaline liquid-rich inclusions, and a scarcity of vapor-rich liquid inclusions suggest that phase separation probably occurred in the source magma chamber. Further phase separation would accompany decompression as the low-density vapor and brine ascended.

6.3 Physical models of magmatic volatile phase separation

Physical models (Shinohara and Kazahaya, 1995; Shinohara et al., 1995; Shinohara and Hedenquist, 1997) for the exsolution of volatiles from a convecting magma body, suggest that at low degrees of crystallization, individual bubbles of magmatic volatile phase formed in the magma will buoyantly rise and coalesce at the top of the magma body. As the volatile concentration increase, the vapor pressure leads to sudden failure of the carapace and adjacent wallrock – this occurs once the vapor pressure is greater than the confining pressure. Magmatic fluids escape as cracking of the wallrock continues; these fluids then hydrothermally alter the rock they pass through. Resealing of the system allows the process to be repeated. As the volume of crystals increases, the residual aqueous fluid becomes trapped. At Bajo de la Alumbrera, each critical stage in the magmatic-hydrothermal transition is recorded: 1) the earliest stage of volatile exsolution, 2) subsequent bubble formation (vesiculation), 3) volatile accumulation, 4) hydrothermal alteration caused by an exsolved magmatic volatile phase.

Silicate-melt and hypersaline liquid-rich inclusions from quartz phenocrysts in the mineralized porphyries preserve the earliest stages of volatile exsolution (e.g., Lowenstern et al., 1991). Previous studies have taken the coexistence of such inclusions to indicate that silicic melt coexisted with hypersaline fluids (Roedder and Coombs, 1967); however, melt/fluid immiscibility is unambiguously preserved by the *composite* silicate-melt inclusions (e.g., Kamenetsky and Naumov 2002; Kamenetsky et al., 2003). In these inclusions a non-silicate volatile-rich hypersaline phase is immiscible with the magma from which it came (e.g., Reyf and

Bazheyev 1977; Frezzotti 1992; Kamenetsky and Naumov, 2002; Kamenetsky et al., 2003). Furthermore, important ore-forming metals, such as Cu, Fe, Pb and Zn, are preferentially partitioned into the associated magmatic volatile phase (Harris et al., 2003b).

At low degrees of crystallization, the evolved magmatic volatile phase is thought to form bubbles in the melt (Candela, 1991). As the magma crystallization proceeds and the viscosity increases, these bubbles coalesce forming tubules through which the volatiles escape upwards. These tubules will ultimately collapse as the volatile supply wanes: they appear in the solidified rock as irregular patches of coarser crystals and aplite. In part, the mineralogy of these textures is similar to the groundmass of the mineralized porphyries. In some granites these tubules are preserved as interconnected miarolitic cavities (Candela and Blevin, 1995). At high degrees of crystallization, the bubbles are more likely to become trapped due to capillary forces; the bubbles cannot ascend until the buoyant forces exceed the capillary force adhering it to the crystal mush (Shinohara and Kazahaya, 1995). These pockets of exsolved fluid remain trapped, unable to escape from the crystal mush. Some miarolitic pods or cavities are preserved examples of these trapped bubbles (Harris et al., 2003a). Evidence for this comes in part from petrographic observations that reveal these quartz eyes as distinct, zoned pockets of saccharoidal quartz and other minerals, including alkali feldspar and hornblende.

Comb quartz layered textures are preserved when an exsolved magmatic volatile phase coalesces and accumulates at the top and sides of the crystallizing magma (Lowenstern and Sinclair, 1996). _-quartz grows from the exsolved magmatic volatile phase, nucleating on aplite bands on the edge of the cooling magma body. Continued degassing of the melt and accumulation of the fluid results in significant overpressure (Lowenstern and Sinclair 1996). Fluid inclusions from the comb quartz layered textures at Bajo de la Alumbrera exhibit homogenisation by halite dissolution, which where observed (e.g., Cline and Bodnar, 1994), has been related to the entrapment of a hypersaline fluid at high temperature and pressure trapping. Over-pressuring ultimately causes fracturing of the carapace, and quartz growth ceases.

Furthermore, rapid under-cooling and devolatilisation of the adjacent magma occurs, causing the formation of a thin aplite band. Fluids draining out of these pockets cause hydrothermal alteration of the adjacent wallrocks (Lowenstern and Sinclair, 1996). Melt may also escape from these pocket, forming thin dyke-like bodies, referred to as vein-dykes – these features are common in many porphyry ore deposits (e.g., Heithersay and Walshe 1995; Lickfold et al., 2003). Repeated volatile exsolution, volatile accumulation, over-pressuring and rupturing of the intrusion carapace and adjacent wallrocks, explains the complex alteration and mineralization patterns that exist in all porphyry ore deposits (Burnham, 1979).

6.4. The magmatic-hydrothermal transition

Recognition of silicate-melt inclusions in transitional magmatic-hydrothermal quartz veins called P veins reflects their primitive role in the evolution of the deposit and unambiguously links devolatilization of the magma with hydrothermal alteration at Bajo de la Alumbrera (Harris et al., 2003b). This occurrence is not surprising given the physical models outlined above; i.e., as bubbles separate, coalesce and grow, small melt droplets become physically entrained in fluids with temperatures up to 845°C. As they cool, the magmatic fluids form hydrothermal minerals, and the melt droplets become trapped as crystallized silicate-melt inclusions.

Available aqueous phase equilibria for fluid inclusions coexisting with silicate-melt inclusions in the transitional P veins yield pressure estimates above 0.7 kbar (Harris et al., 2003b). By contrast, the bulk of the fluid inclusions from more typical, lower temperature hydrothermal alteration assemblages have pressures of 0.3 kbar. Consequently, the magmatic volatile phase (+ melt) responsible for the P veins has been interpreted to have exsolved while the confining carapace was still intact (Harris et al., 2003b). Instead of melt, as in the case of the vein-dykes, magmatic volatiles are now the dominant fluid phase being squeezed out of the magma (melt + crystals). Once the internal fluid pressure exceeds the confining pressure (i.e., > 0.7 kbar), the carapace and overlying rock column ruptures. Catastrophic decompression would

cause sudden foaming of the magma, with rapid bubble growth. Decompression also results in pressure quenching of the magma and release of all remaining magmatic volatile phase in the upper parts of the magma body (Burnham, 1979). Burnham (1979) also stated that decompression of the magma invariably causes the system to close by mineral deposition, causing magmatic volatiles to start to accumulate again.

It is probable that earliest Cu deposition at Bajo de la Alumbrera resulted from the failure of the rock column (Harris et al., 2003b). Simultaneous with this failure is boiling of the early-formed vapor and hypersaline fluid phases. As these magmatic volatile phase escape outwards into the wallrock (i.e., a predominantly hydrostatic regime), any change in temperature, pH and/or oxygen fugacity of the system would have caused Cu-Fe sulfides to deposit from the residual brines (Hezarkhani and Willims-Jones, 1998; Ulrich et al., 2002; Harris et al., 2003b).

7. Implications and Conclusions

Quartz in the porphyries at Bajo de la Alumbrera preserves evidence of the earliest stages of exsolution, bubble formation (vesiculation), and volatile accumulation, culminating in hydrothermal alteration caused by magmatic aqueous fluids. Preservation of interconnected miarolitic cavities, together with their mineralogy and magmatic inclusion petrography, in mineralized porphyries at Bajo de la Alumbrera imply that: 1.) the intrusions were once a dynamic mixture of crystals and magmatic volatile phases consisting of gas and high-temperature brine in the melt (i.e., an effervescing magma; Burnham, 1979); 2.) that the magmatic volatile phase was rich in H_2O, Cl, SO_2, SO_3, and Cu; 3.) droplets of melt were physically entrained into the magmatic volatile phase at the time of separation; and 4.) the intrusions had considerable permeability (Candela and Blevin, 1995) through which the magmatic volatile phase could stream upwards. The ability to recognize textural features, such as interconnected miarolitic cavities, may provide a useful tool for mineral exploration. Recognition of these textures, including the associated quartz segregations (or quartz eyes) during field

observations may provide immediate evidence for a potentially fertile magmatic system that exsolved, accumulated and released a magmatic volatile phase to the adjacent wallrock.

Acknowledgments

The Centre for Ore Deposit Research, University of Tasmania directly funded this work. The first author would like to thank Shunso Ishihara for the opportunity to contribute to this volume, and Phil Belvin for his encouragement. Sample material used during this study, was collected as part of the first author's doctoral research at The University of Queensland, funded by an Australian Postgraduate Award scholarship. MIM Exploration (now Xstrata) and Minera Alumbrera are thanked for financial and logistical support and access to the Farallón Negro district during the first author's doctoral research. We thank John Proffett for his ongoing detailed reviews of our work. Three anonymous reviewers are thanked for their constructive comments that helped refine the manuscript.

References

Ahmad, S. N. and Rose, A. W. (1980) Fluid inclusions in porphyry and skarn ore at Santa Rita, New Mexico. Econ. Geol., 75, 229-250.

Beane, R. E. and Titley, S. R. (1981) Porphyry copper deposits; Part II, Hydrothermal alteration and mineralization. *in* Skinner, B .J. (ed.) Economic geology; 75th Anniversary Volume, 235-269.

Bodnar, R. J. (1995) Fluid-inclusions evidence for a magmatic source of metals in porphyry copper deposits. *in* Thompson J. F. H. (ed), Magmas, Fluids and Ore Deposits. Miner. Assoc. Canada Short Course Ser., 139-152.

Burnham, C. W. (1979) Magmas and hydrothermal fluids, *in* Barnes, H.L. (ed.) Geochemistry of Hydrothermal Ore Deposits, 2nd ed., New York, Wiley, 71-136.

Burnham, C. W. (1981) Physicochemical constraints on porphyry mineralization. Geological Society of Arizona Digest, 14, 71-77.

Burnham, C. W. and Ohmoto, H. (1980) Late-stage processes of felsic magmatism. Mining Geol. Special Issue 8, 1-11.

Candela, P. A. (1989) Felsic magmas, volatiles, and metallogenesis. Reviews in Economic Geology, 4, 223-233.

Candela, P. A. (1991) Physics of aqueous phase evolution in plutonic environments. Amer. Mineral., 76, 1081-1091.

Candela, P. A. (1994) Combined chemical and physical model for plutonic devolatilisation: A non-Rayleigh fractionation algorithm. Geochim. Cosmochim. Acta, 58, 2157-2167.

Candela, P. A. and Blevin, P. L. (1995) Do some miarolitic granites preserve evidence of magmatic volatile phase permeability? Econ. Geol., 90, 2310-2316.

Candela, P. A. and Holland, H. D. (1984) The partitioning of copper and molybdenum between silicate melts and aqueous fluids: Geochim. Cosmochim. Acta, 48, 373-380.

Candela, P. A. and Piccoli, P. M. (1995) Model ore-metal partitioning from melts into vapor and vapor-brine mixtures: Mineralogical Association of Canada Short Course Series 23, 101-127.

Carten, R. B., Geraghty, E. P., Walker, B. M. and Shannon, J. R. (1988) Cyclic development of igneous features and their relationship to high-temperature hydrothermal features in the Henderson porphyry molybdenum deposit, Colorado. Econ. Geol., 83, 266-296.

Carroll, M. R. and Rutherford, M. J. (1987) The stability of igneous anhydrite: Experimental results and implications for sulfur behaviour in the 1982 El Chichon trachyandesite and other evolved magmas. Jour. Petrol., 28, 781-801.

Cline, J. S. and Bodnar, R. J. (1994) Direct evolution of brine from a crystallizing silicic melt at the Questa, New Mexico, molybdenum deposit. Econ. Geol., 89, 1780-1802.

Coughlin, T. J., O'Sullivan, P. B., Kohn, B. P. and Holcombe, R. J. (1998) Apatite fission-track thermochronology of the Sierras Pampeanas, central western Argentina: Implications for the mechanism of plateau uplift in the Andes. Geology, 26, 999-1002.

de Urreiztieta, M., Gapais, D., Le, C. C., Cobbold, P. R., Rossello, E. (1996) Cenozoic dextral transpression and basin development at the southern edge of the Puna Plateau, northwestern Argentina. Tectonophys., 254,17-39.

Dilles, J. H. (1987) Petrology of the Yerington Batholith, Nevada: Evidence for evolution of porphyry copper ore fluids. Econ. Geol., 82, 1750-1789.

Eastoe, C. J. (1978) A fluid inclusion study of the Panguna porphyry copper deposit, Bougainville, Papua New Guinea. Econ. Geol., 73, 721-748.

Frezzotti, M. L. (1992) Magmatic immiscibility and fluid phase evolution in the Mount Genis granite (southeastern Sardinia, Italy). Geochim. Cosmochim. Acta, 56, 21-33.

Guilbert, J. M. (1995) Geology, alteration, mineralization and genesis of the Bajo de la Alumbrera porphyry copper-gold deposit, Catamarca province, Argentina. Arizona Geological Society Digest, 20, 646-656.

Gustafson, L. B. and Hunt, J. P. (1975) The porphyry copper deposit at El Salvador, Chile. Econ. Geol., 70, 857-912.

Harris, A. C. (2002) The Genesis of a Porphyry Cu-Au Deposit, Farallón Negro Volcanic Complex, NW Argentina. Unpublished Ph.D. Thesis, The University of Queensland, 281p.

Harris, A. C., Kamenetsky, V. S., and White, N.C. (2003a) Immiscible magmatic volatiles in the Bajo de la Alumbrera Cu-Au porphyries: Melt and fluid inclusions record in quartz eyes. *in* Mineral Exploration and Sustainable Development. The 7th Biennial Meeting, 24-28 August 2003. Society for Geology Applied to Mineral Deposits. 275-278.

Harris, A. C., Kamenetsky, V. S., White, N. C., van Achterbergh, E. and Ryan, C. G. (2003b) Silicate-melt inclusions in quartz veins: Linking magmas and porphyry Cu deposits. Science, 302, 2109-2111.

Harris, A. C., Allen, C. A., Bryan, S. E., Campbell, I. H., Holcombe, R. J. and Palin, M.J. (2004) Measuring the longevity of regional volcanism hosting the Bajo de la Alumbrera Cu-Au deposit: Implications for the genesis of porphyry ore deposits. Mineral. Deposita, 39, 46-67.

Haynes, F. M. and Titley, S. R. (1980) The evolution of fracture-related permeability within the Ruby Star Granodiorite, Sierrita porphyry copper deposit, Pima County, Arizona. Econ. Geol., 75, 673-683.

Heithersay, P. S. and Walshe, J. L. (1995) Endeavour 26 North: A porphyry copper-gold deposit in the Late Ordovician shoshonitic Goonumbla Volcanic Complex, New South Wales, Australia. Econ. Geol., 90, 1506-1532.

Hedenquist, J. W. and Lowenstern, J. B. (1994) The role of magmas in the formation of hydrothermal ore deposits. Nature 370, 519-527.

Hedenquist, J. W., Arribas, A. and Reynolds, T. J. (1998) Evolution of an intrusion-centered hydrothermal system: Far Southeast Lepanto porphyry and epithermal Cu-Au deposits, Philippines. Econ. Geol., 93, 374-404.

Hezarkhani, A. and Willims-Jones, A.E. (1998) Controls of alteration and mineralization in the Sungun porphyry copper deposit, Iran: Evidence from fluid inclusions and stable isotopes. Econ. Geol., 93, 651-670.

Jahns, R. H. and Burnham, C. W. (1969) Experimental studies of pegmatite genesis; l, A model for the derivation and crystallization of granitic pegmatites. Econ. Geol., 64, 843-864.

Johnson, M. C., Anderson, A. T. Jr. and Rutherford, M. J. (1994) Pre-eruptive volatile contents of magmas. *in* Volatiles in Magmas. Heaney, P. J., Prewitt, C. T., and Gibbs, G. V. (eds.) Reviews in Mineralogy 30, 281-330.

Jordan, T. E. and Allmendinger, R. W. (1986) The Sierras Pampeanas of Argentina: A modern analogue of Rocky Mountain foreland deformation. Amer. Jour. Sci., 286,737-764.

Jordan, T. E, Isacks, B. L., Allmendinger, R. W., Brewer, J. A., Ramos, V. A. and Ando, C. J. (1983) Andean tectonics related to geometry of subducted Nazca Plate. Geol. Soc. Amer. Bull., 94, 341-361

Kamenetsky, V. S. and Naumov, V. B. (2002) Melt immiscibility in granite: A "missing link: in magmatic-hydrothermal transition. Goldschmidt Conference Abstracts, Geochim. Cosmochim. Acta, 66 (Supplement 1), A379.

Kamenetsky, V. S., Wolfe, R. C., Eggins, S. M., Mernagh, T. P., and Bastrakov, E. (1999) Volatile exsolution at the Dinkidi Cu-Au porphyry deposit, Philippines: A melt-inclusions record of the initial ore-forming process. Geology, 30, 691-694.

Kamenetsky, V. S., De Vivo, B., Naumov, V. B., Kamenetsky, M. B., Mernagh, T. P., Van Achterbergh, E., Ryan C. G., Davidson, P., (2003) Magmatic inclusions in the search for natural silicate-salt melt immiscibility: Methodology and example. *in* De Vivo, B., and Bodnar, R.J. (eds.) Melt Inclusions in Volcanic Systems: Methods, Applications and Problems. Developments in Volcanology 5. 65-82.

Kirkham, R. V. and Sinclair, W. D. (1988) Comb quartz layers in felsic intrusions and their relationship to porphyry deposits. *in* Taylor, R. P., and Strong, D. F. (eds.) Recent Advances in the Geology of Granite-related Mineral Deposits. 50-71, Canadian Institute of Mining and Metallurgy Special Volume 39, Montreal, Canada.

Kirwin, D. J. and Seltmann, R. (2002) Unidirectional solidification textures associated with intrusion-related gold deposits. *in* 11th Quadrennial IAGOD Symposium and GEOCONGRESS 2002, 22-26 July 2002. 31.

Knight, C. L., and Bodnar, R. J. (1989) Synthetic fluid inclusions; IX, Critical PVTX properties of NaCl-H_2O solutions. Geochimica et Cosmochimica Acta, 53, 3-8.

Lickfold, V., Wilson, A., Harris, A. C. and Cooke, D. R. (2003) The alkalic Au-Cu porphyry deposits of NSW, Australia: Evidence for coexisting melt and hydrothermal fluids in comb quartz layers. *in* Mineral Exploration and Sustainable Development. The 7th Biennial Meeting, 24-28 August 2003. Society for Geology Applied to Mineral Deposits. 315-318.

Lowell, J. D. and Guilbert, J. M. (1970) Lateral and vertical alteration-mineralization zoning in porphyry ore deposits. Econ. Geol., 65, 373-408.

Lowenstern, J. B. (1994) Chlorine, fluid immiscibility, and degassing in peralkaline magmas from Pantelleria, Italy. Amer. Mineral., 79, 353-369.

Lowenstern, J. B. and Sinclair, W. D. (1996) Exsolved magmatic fluid and its role in the formation of comb-layered quartz at the Cretaceous Logtung W-Mo deposit, Yukon Territory, Canada. Transactions of the Royal Society of Edinburgh: Earth Sciences 87, 291-303.

Lowenstern, J. B., Mahood, G. A. Rivers, M. L. and Sutton, S. R. (1991) Evidence for extreme partitioning of copper into a magmatic vapor phase. Science, 252, 1405-1408.

McDougall, I. and Harrison, T. M. (1999) Geochronology and Thermochronology by the $^{40}Ar/^{39}Ar$ Method, 2 edn. Oxford University Press, New York 269 p.

Metrich, N. and Rutherford, M. J. (1992) Experimental study of chlorine behavior in hydrous silicic melts. Geochim. Cosmochim. Acta, 56, 607-616.

Müller, D. and Forrestal, P. (1998) The shoshonite porphyry Cu-Au association at Bajo de la Alumbrera, Catamarca Province, Argentina: Contrib. Mineral. Petrol., 64, 47-64.

Nakada, S. (1991) Magmatic processes in titanite-bearing dacites, Central Andes of Chile and Bolivia. Amer. Mineral., 76, 548-560.

Pasteris, J. D. (1996) Mount Pinatubo volcano and "negative" porphyry copper deposits. Geology, 24, 1075-1078.

Penniston-Dorland, S. C. (2001) Illumination of vein quartz textures in a porphyry copper ore deposit using scanned cathodoluminescence; Grasberg igneous complex, Irian Jaya, Indonesia. Amer. Mineral., 86, 652-666.

Proffett, J. M. (1995) Geology of the Bajo de la Alumbrera porphyry Cu-Au deposit, Catamarca Province, Argentina: Unpub. Minera Alumbrera Ltd. Internal Report, 85 p.

Proffett, J. M. (1997) Geology of the Bajo de la Alumbrera porphyry Cu-Au deposit, Catamarca Province, Argentina: Unpub. Minera Alumbrera Internal Report, 169 p.

Proffett, J. M. (2003) Geology of the Bajo de la Alumbrera porphyry copper-gold deposit, Argentina. Econ. Geol. 98, 1535-1574.

Ramos, V. A., Reynolds, J. H., Jordan, T. E. and Tabbutt, K. D. (1988) Time constraints for the uplift of the Sierras de Toro Negro, Umango, and Espinal, western Sierras Pampeanas, Argentina. Geological Society of America Abstracts with Programs 20, 61.

Reyf, F. R. and Bazheyev, Y. D. (1977) Magmatic chloride solutions and tungsten mineralization. Geochemistry International 14, 45-51.

Reynolds, J. H., Tabbutt, K. T., Johnson, N. M., and Jordan, T. E. (1987) Non-systematic uplift of the northwestern Sierras Pampeanas, Catamarca Province, Argentina: Interpretation of magnetic polarity stratigraphy data. Geological Society of America Abstracts with Programs 19, 817.

Roedder, E. (1992) Fluid inclusion evidence for immiscibility in magmatic differentiation. Geochimica et Cosmochimica Acta, 56, 5-20.

Roedder, E. and Coombs, D. S. (1967) Immiscibility in granitic melts, indicated by fluid inclusions in ejected granitic blocks from Ascension island. Jour. Petrol., 8, 417-449.

Sasso, A. M. and Clark, A. H. (1998) The Farallón Negro group, northwest Argentina: magmatic, hydrothermal and tectonic evolution and implications for Cu-Au metallogeny in the Andean back-arc. Society of Economic Geologists Newsletter 34:1, 8-18

Sheppard, S. M. F. and Gustafson, L. B. (1976) Oxygen and hydrogen istoles in the porphyry copper deposit at El Salvador, Chile. Econ. Geol., 71, 1549-1559.

Shinohara, H. (1994) Exsolution of immiscible vapor and liquid phases from a crystallizing silicate melt: Implications for chlorine and metal transport. Geochim. Cosmochim. Acta, 58, 5215-5221.

Shinohara, H. and Kazahaya, K. (1995) Degassing processes related to magma-chamber crystallization. Mineralogical Association of Canada Short Course Series 23, 47-70.

Shinohara, H. and Hedenquist, J. W. (1997) Constraints on magma degassing beneath the Far Southeast porphyry Cu-Au deposit, Philippines. Jour. Petrol. 38, 1741-1752.

Shinohara, H., Kazahaya, K., and Lowenstern, J. B. (1995) Volatile transport in a convecting magma column; implications for porphyry Mo mineralization. Geology, 23, 1091-1094.

Stults, A. (1985) Geology of the Bajo de la Alumbrera Porphyry Copper and Gold Prospect, Catamarca Province, Argentina: M.Sc. Thesis, University of Arizona, 75 p.

Strecker, M. R., Cerveny, P., Bloom, A. L. and Malizia, D. (1989) Late Cenozoic tectonism and landscape development in the foreland of the Andes; northern Sierras Pampeanas (26 degrees - 28 degrees S), Argentina. Tectonics, 8, 517-534.

Strecker, M. R., Bloom, A. L. and Malizia, D. (1990) Neotectonic activity in the northern Sierras Pampeanas, Argentina: Colloques et Seminaires - Institut de Recherche Scientifique pour le Developpement en Cooperation, Paris, 99-102.

Tabbutt, K., Naeser, C. W., Jordan, T. E. and Cerveny, P. F. (1987) Edades nuevas por metodo de trazas de fision de todas Mio-Pliocene en las sierras Pampeanas y la Precordillera de Argentina. Actas del Congreso Geologico Argentino, 4, 222-224.

Ulrich, T. and Heinrich, C. A. (2002) Geology and alteration geochemistry of the porphyry Cu-Au deposit at Bajo de la Alumbrera, Argentina. Econ. Geol., 96, 1719-1742.

Ulrich, T., Günthur, D. and Heinrich, C. A. (2002) The evolution of a porphyry Cu-Au deposit, based on LA-ICP-MS analysis of fluid inclusions: Bajo de la Alumbrera, Argentina. Econ. Geol., 96, 1743-1774.

Webster, J.D. (1992) Water solubility and chlorine partitioning in Cl-rich granite systems: Effects of melt composition at 2 kbar and 800°C. Geochim. Cosmochim. Acta, 56, 679-687.

Webster, J. D., (1997) Chloride solubility in felsic melts and the role of chloride in magmatic degassing. Jour. Petrol., 38, 1793-1807.

Williams, T. J., Candela, P. A. and Piccoli, P. M. (1995) The partitioning of copper between silicate melts and two-phase aqueous fluids; an experimental investigation at 1 kbar, 800 degrees C and 0.5 kbar, 850 degrees C: Contributions to Mineralogy and Petrology, 121, 388-399.

Wilson, J. W., Kesler, S. E., Cloke, P. L. and Kelly, W. C. (1980) Fluid inclusion geochemistry of the Granisle and Bell porphyry copper deposits, British Columbia. Econ. Geol., 75, 45-61.

Yang, K. and Bodnar, R. J. (1994) Magmatic-hydrothermal evolution in the "bottoms" of porphyry copper systems: Evidence from silicate melt and aqueous fluid inclusions in granitoid intrusions in the Gyeongsang Basin, South Korea. International Geology Review, 36, 608-628.

Figures

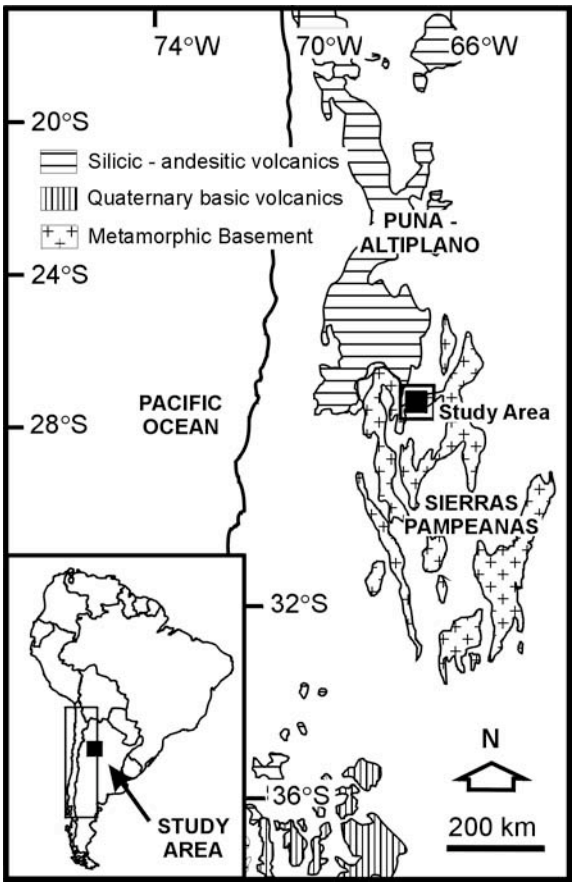

Fig. 1. Geologic outline map of the central volcanic zone (modified after Jordan et al., 1983, Ulrich and Heinrich, 2002).

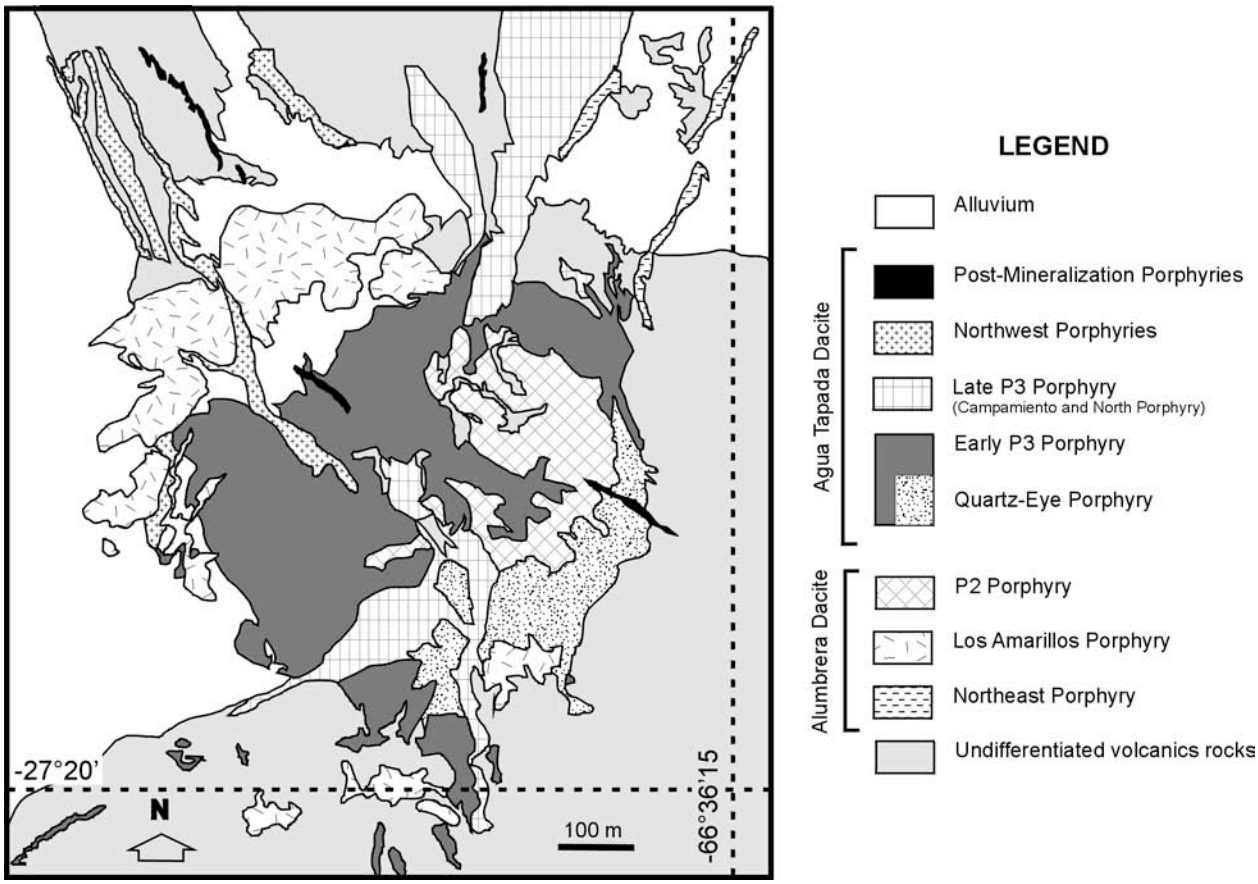

Fig. 2. Geology of Bajo de la Alumbrera (Ulrich and Heinrich, 2002; complied from mapping of Proffett, 1995, 1997, 2003 and incorporating nomenclature from Harris et al., 2004).

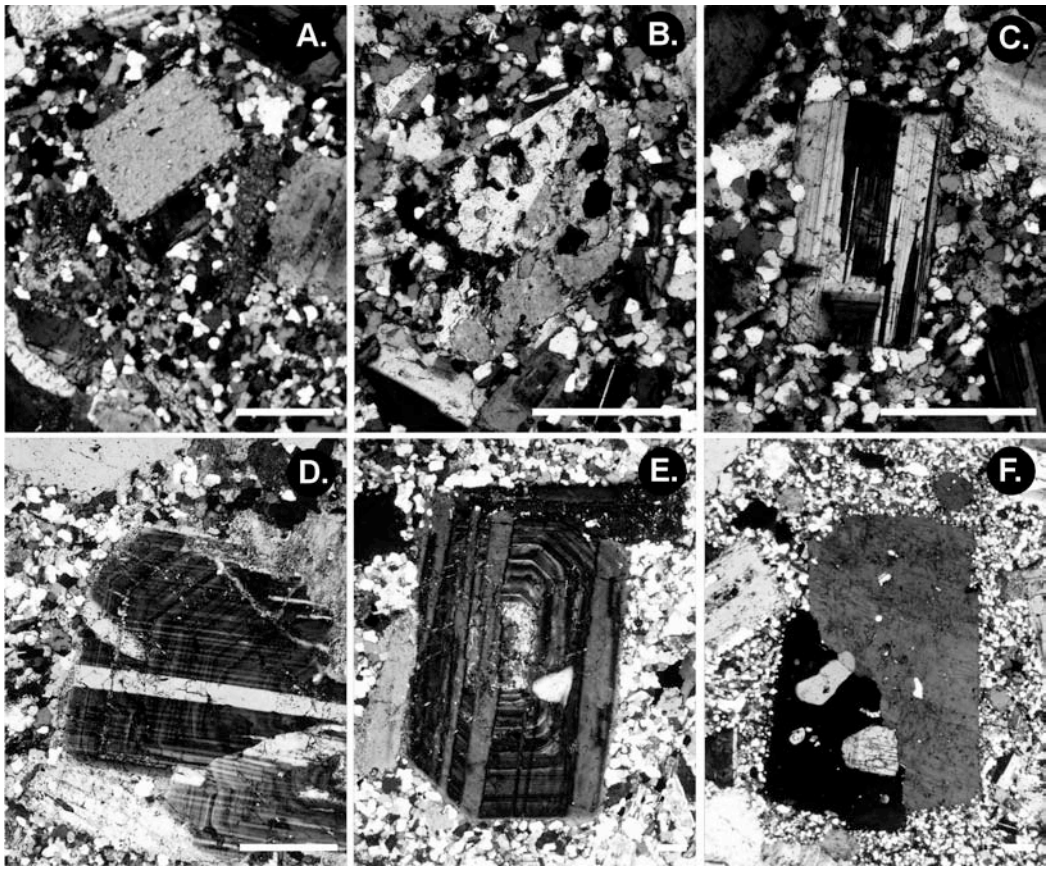

Fig. 3. Representative igneous phenocrysts in the mineralized porphyries at Bajo de la Alumbrera (Late P3 and Northwest Porphyries). A. Biotite phenocryst surrounded by quartzo-feldspathic groundmass. B. Euhedral hornblende poikilitically enclosing magnetite. C. Distinctly twinned euhedral plagioclase. D. Zoned plagioclase. E. Zoned plagioclase with some internal discontinuity in the growth bands. The plagioclase also poikilitically encloses quartz and has an altered, presumably calcic core. F. Distinct alkali feldspar phenocryst poikilitically enclosing quartz and finer grained quartz and feldspar. Scale bars are 100_m.

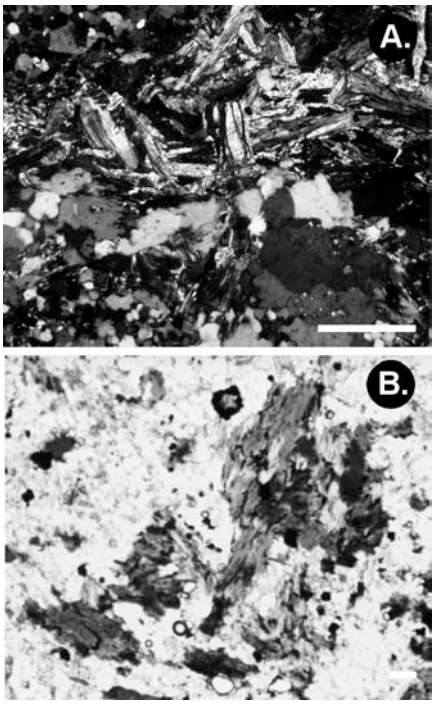

Fig. 4. Secondary biotite (potassic) alteration at Bajo de la Alumbrera (P2 Porphyry). A. Fracture controlled shredded biotite (cross polarized light). B. Shredded biotite intergrown with magnetite. Trails of fine shredded biotite demonstrate a clear fracture-controlled and overprinting relationship to this biotite and therefore the alteration. Scale bars are 100_m.

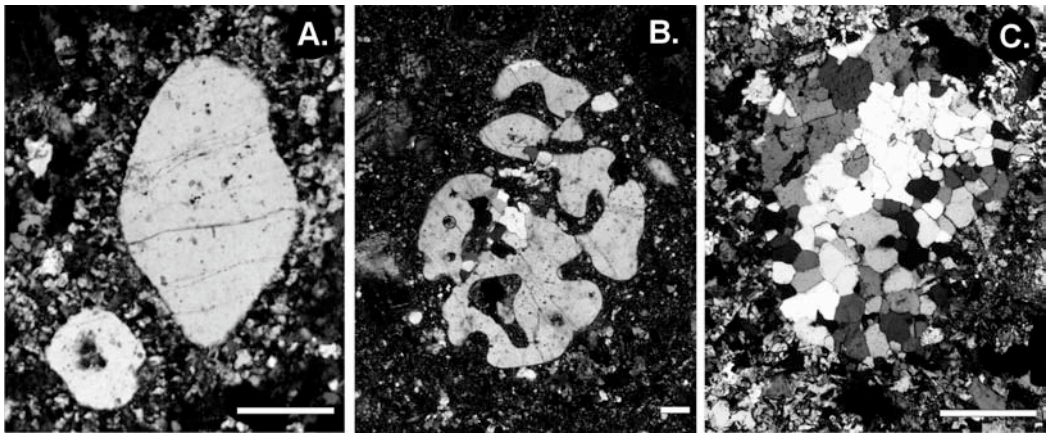

Fig. 5. Quartz eyes in dacite porphyries (Early P3 Porphyry) from Bajo de la Alumbrera. A. Type 1 quartz eyes or phenocrysts. B. Some Type 1 quartz phenocrysts have an amoeboid appearance because of embayments. C. Type 2 quartz eyes appearing as polycrystalline quartz aggregates. Note that these types of quartz eyes occur in interconnected miarolitic cavities (see Fig. 6). Scale bars are 100_m.

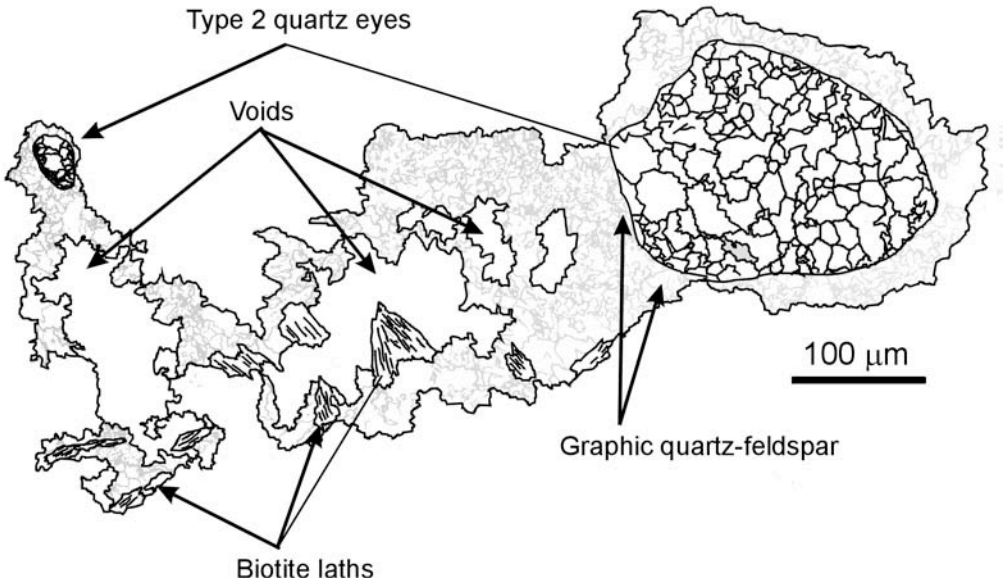

Fig. 6. Sketch of interconnected miarolitic cavity. Sample from Minera Alumbrera diamond drill hole 50-46.43 from 613.2m depth. Scale bars are 100_m.

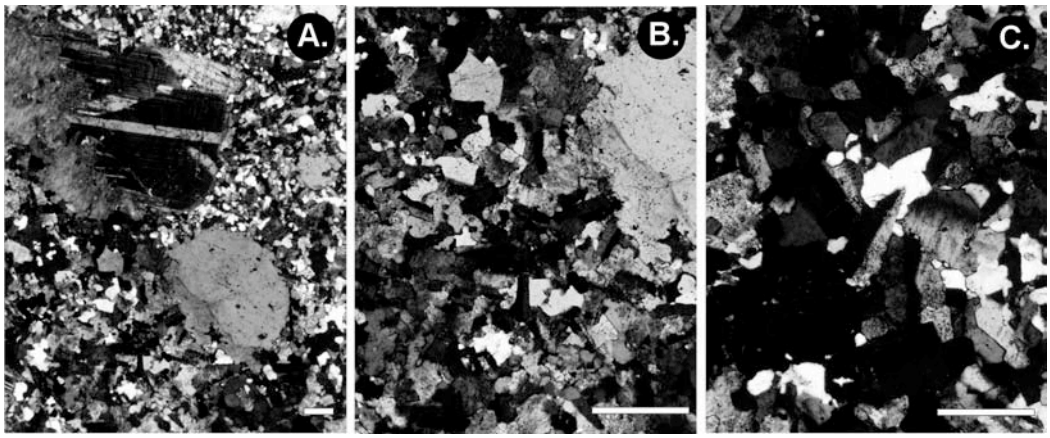

Fig. 7. Photomicrographs of two-domain or ‘double bunger’ texture (Candela and Blevin, 1995; P. Blevin pers. comm., 2003). A. Coarser grained aplite of the interconnected miarolitic cavity (bottom left) contrasts the more typical finer grained groundmass of the porphyry (top right). Also shown is the intergrowth of alkali feldspar of the interconnected miarolitic cavity and a plagioclase phenocryst along the edge of the tubular structure. B. Prismatic and sugary quartz and alkali feldspar intergrowths interconnect the sugary pods of the miarolitic cavity. C. Intergrowths of quartz and alkali feldspar exhibit typical aplitic textures. Scale bars are 100_m.

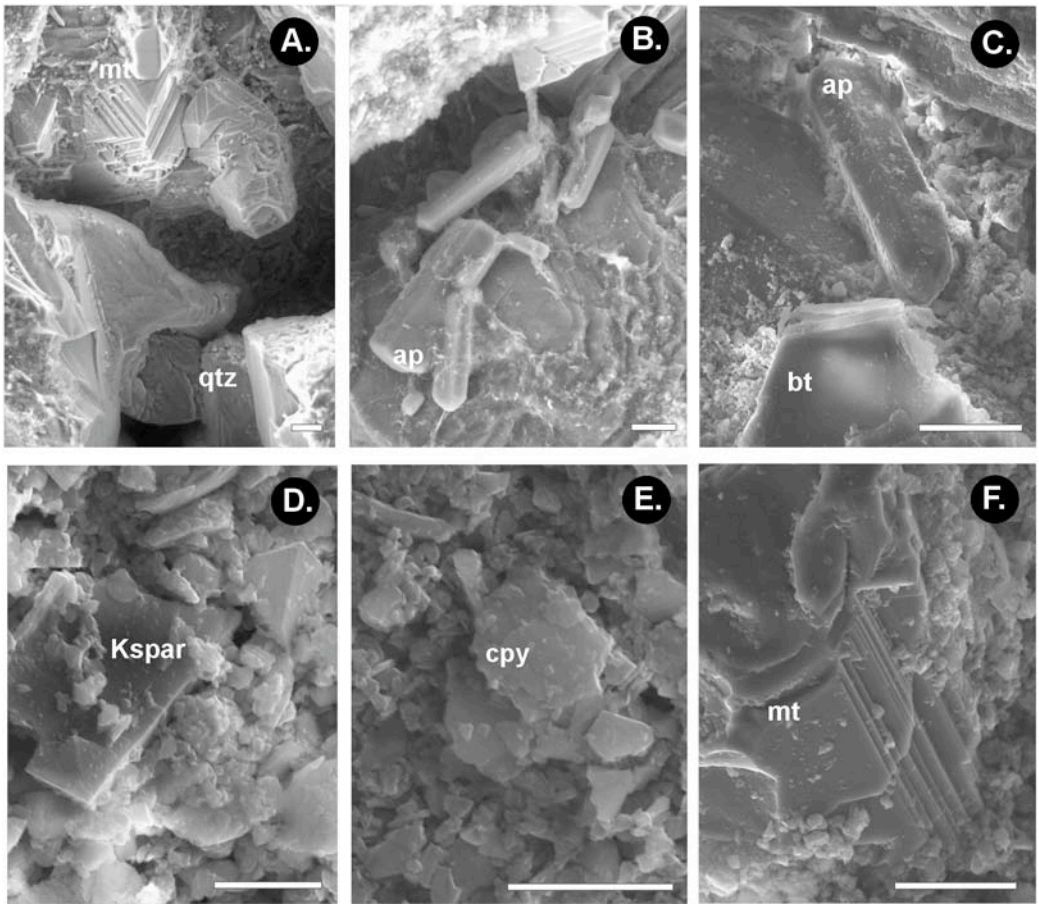

Fig. 8. SEM photomicrographs of interconnected miarolitic cavities (Late P3 Porphyry). A-F. Examples of subhedral to euhedral quartz (qtz), magnetite (mt), apatite (ap), biotite (bt), and chalcopyrite (cpy) that line the walls of an interconnected miarolitic cavity and terminate in voids. Secondary electron images were collected using an ElectroScan ESEM2020 scanning electron microscope operated at an accelerating voltage of 20kV. Fig. 8a and b were acquired in ESEM environmental mode on uncoated samples using water as the imaging medium at 5 torr chamber pressure. Fig. 8c-f were acquired from carbon coated samples in ESEM high vacuum mode. Scale bars are 10_m.

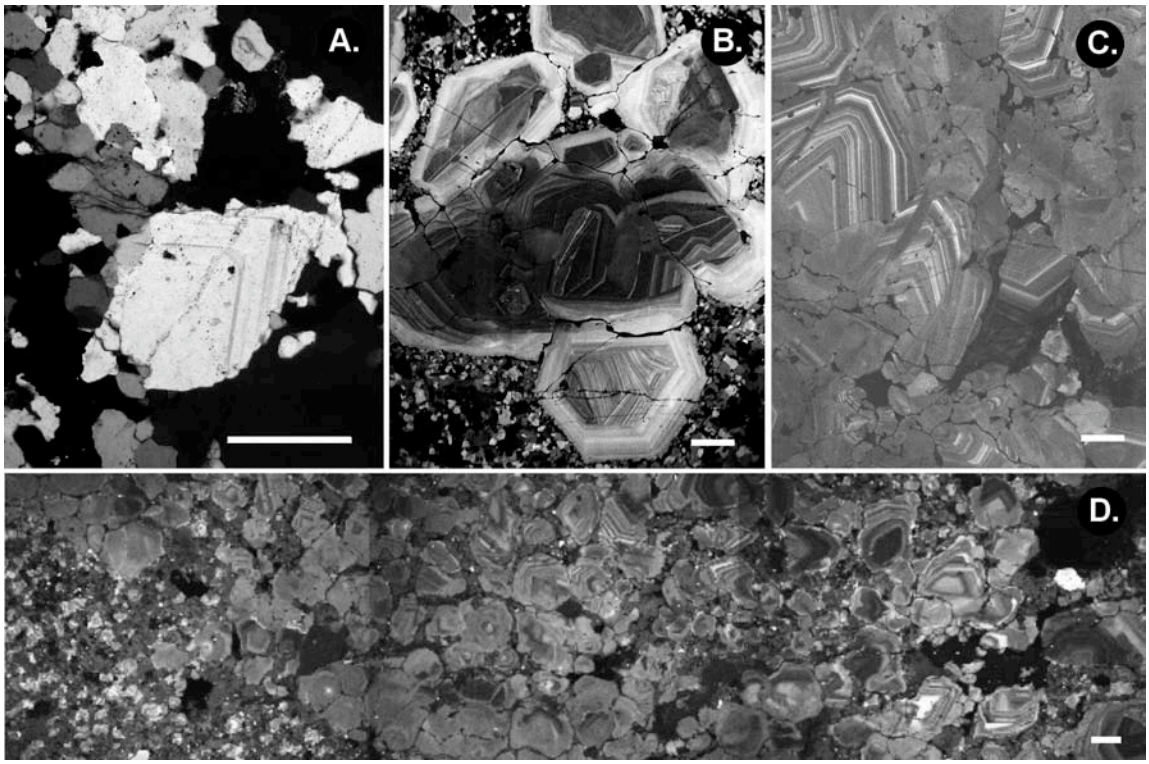

Fig. 9. Quartz in comb-quartz layered textures and transitional magmatic-hydrothermal quartz P veins. A. Prismatic quartz crystal, with distinct primary fluid inclusion trails, in comb-quartz layered texture (contact of Late P3 Porphyry). B. Scanning cathodoluminescence image of prismatic quartz in comb-quartz layered textures. Note the complex resorption and overgrowth patterns and that the quartz is bipyramidal, indicative of β-quartz. C. Cathodoluminescence image of narrow bands of prismatic quartz typical of comb-quartz layered textures. The growth direction is towards the top right corner of the image. These prismatic terminations are directed towards the related intrusion. D. Cathodoluminescence image of a P vein (cutting P2 Porphyry), which crosses from the bottom right to the top left of the image. Despite being optically continuous, the vein comprises bipyramidal saccharoidal quartz. Panchromatic cathodoluminescence images were acquired on a Cameca SX100 electron microprobe operated at 10kV accelerating voltage and 100nA (faraday cup) beam current. Scale bars are 100_m.

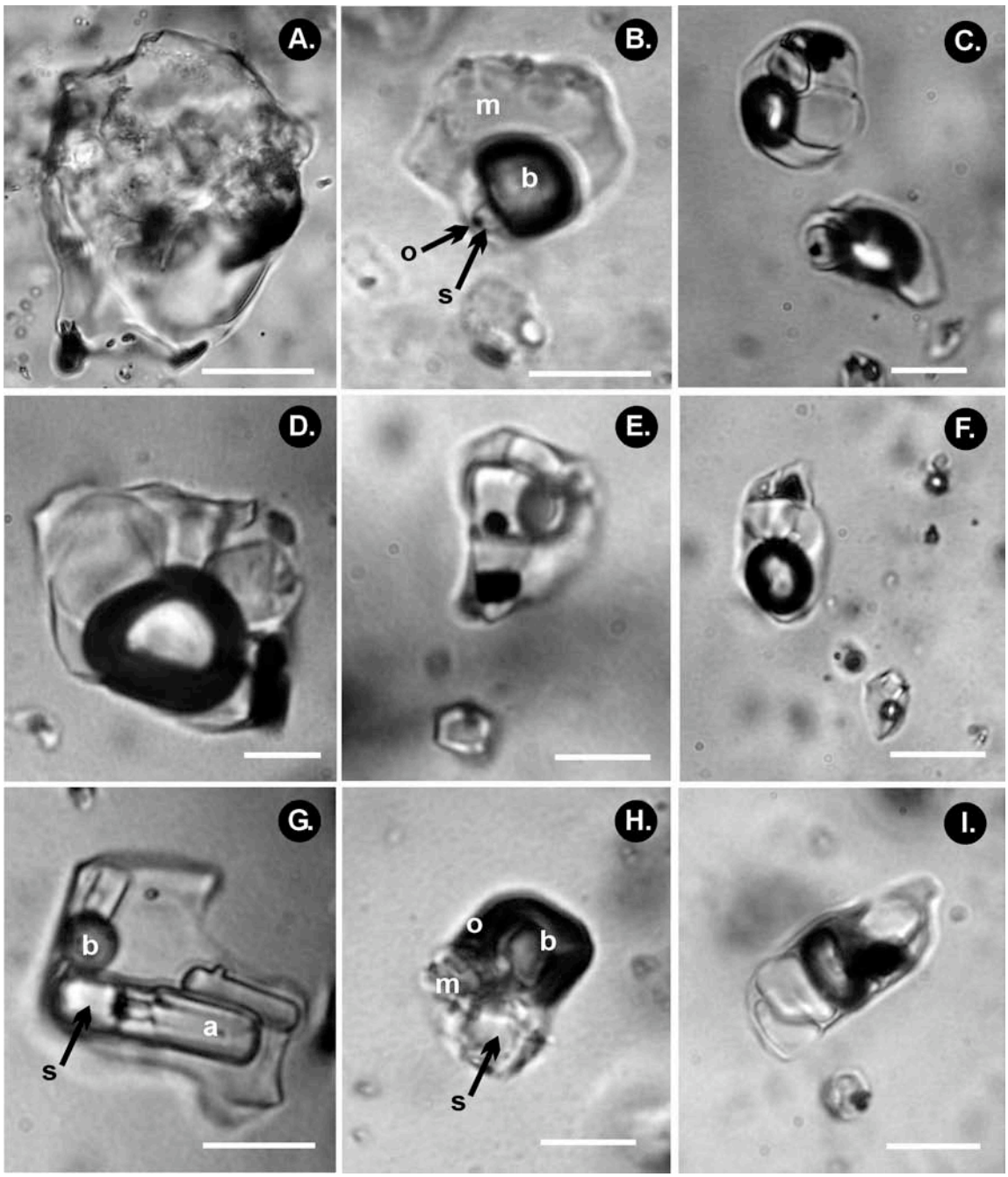

Fig. 10. Magmatic inclusion populations in magmatic quartz at Bajo de la Alumbrera. A. Silicate-melt inclusion in type 1 quartz eyes (Early P3 Porphyry). B. Heated and quenched volatile-rich silicate-melt inclusion with distinct volatile-rich globule containing a large vapour bubble (b), cubic salt (s), and an opaque (o) daughter crystal, surrounded by homogenized silicate glass (g). C. Polyphase brine and high-density vapour-rich fluid inclusions that coexist with silicate-melt inclusions in type 1 quartz eyes. D. Polyphase brine fluid inclusion in comb-quartz layered texture. Note that the inclusion is crowded with salts and opaque crystals (probably oxides and sulfides). E. Primary inclusions in comb-quartz layered textures (contact of Late P3 Porphyry). Note multiple opaque phases and the distinct halite cube. F. A primary inclusion trail in comb-quartz layered texture. In these inclusions, a distinct triangular chalcopyrite crystal is clearly visible. G. Apatite (a) bearing fluid inclusion in comb-quartz layered texture. H. Silicate-melt inclusion in P vein. (cutting P2 Porphyry). I. Polyphase high-temperature (~815°C) fluid inclusion in P vein Scale bars are 10_m.

Table 1. Summary of magmatic inclusions in quartz from dacite porphyries at Bajo de la Alumbrera (modified after Harris et al., 2003a,b).

Inclusion Group		Description	Distribution
	*1A: Volatile-rich silicate-melt*	Melt-vapour-salt(s) ± cpy.-mt.	Found as primary inclusions in quartz eyes (Type 1 and 2), interconnected miarolitic cavities and comb-quartz layered textures. Also occur as clusters in P veins. Coexists with group II and III inclusions. They also appear as primary inclusions in comb-quartz layered quartz textures. In this case, they coexist with group II inclusions.
	1B: Silicate-melt	Melt-vapour ± opaque (?cpy.)	Rare in primary inclusion trails in quartz eyes (Type 1 and 2). Isolated inclusions.
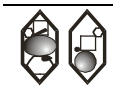	*II: Hypersaline liquid-rich*	Salt(halite-sylvite)-vapour-liquid ± cpy.-mt. (hem.)	Occurring in quartz eyes and comb-quartz layered textures. More commonly seen in primary and secondary inclusion trails in potassic alteration assemblages. Coexists with group III inclusions.
	*III: Low density vapour-rich*	Vapour-opaque (?cpy.) ± liquid	Abundant in primary inclusion trails in some quartz eyes; however, these inclusions are less abundant than group II inclusions.

Melt = small silicate aggregates observed at room temperatures
Abbreviations: cpy. = chalcopyrite; mt. = magnetite; hem. = hematite.